Energy 51 (2013) 154–162

Contents lists available at SciVerse ScienceDirect

Energy

journal homepage: www.elsevier.com/locate/energy

Two fuzzy-based direct power control strategies for doubly-fed induction generators in wind energy conversion systems

Mohammad Pichan [a,*], Hasan Rastegar [a], Mohammad Monfared [b]

[a] Department of Electrical Engineering, Amirkabir University of Technology, P.O. Box: 15875-4413, Tehran, Iran
[b] Department of Electrical Engineering, Ferdowsi University of Mashhad, Mashhad, Iran

ARTICLE INFO

Article history:
Received 21 July 2012
Received in revised form
8 November 2012
Accepted 27 December 2012
Available online 8 February 2013

Keywords:
(Direct power control) DPC
(Fuzzy logic controller) FLC
(Doubly fed induction generator) DFIG

ABSTRACT

This paper proposes two novel (direct power control) DPC strategies for a doubly fed induction generator (DFIG)-based wind energy conversion system based on a (fuzzy logic controller) FLC. At first, the mathematical model of the DFIG in the synchronous reference frame is derived. Then, based on this model, two novel FLC-based DPC strategies, called (fuzzy-based DPC) FDPC and (fully fuzzy-based DPC) FFDPC are proposed. In the FDPC, the required rotor voltages to eliminate power errors within each fixed sampling period are directly calculated based on the FLC, the measured active and reactive powers, the stator voltage and some machine parameters. On the other hand, in the FFDPC, the rotor voltages are directly calculated from the FLC. The control structures of proposed methods are very simple. Compared to the conventional switching table-based DPC, in the proposed methods, the hysteresis comparator and the switching table are replaced by a simple FLC and a PWM (pulse width modulation) modulator. The converter switching frequency is constant which simplifies the practical implementation. Also the proposed methods are robust against machine parameters mismatches and grid voltage disturbances. Extensive simulations in Matlab\Simulink are performed to confirm the effectiveness of the proposed methods under transient and steady state conditions.

1. Introduction

With increasing concerns about the world's fossil fuel reserves as well as CO_2 emissions, renewable energy sources have found more attention. Especially wind energy has become an important source for electricity generation in many countries and it is expected that wind energy will provide more electrical energy in future [1–3].

Variable speed wind energy conversion systems are implemented with either doubly fed induction generators [4] or full power converters [5,6]. Nowadays, many wind farms are based on the (doubly fed induction generator) DFIG technology with converters rated at 20%–30% of the generator rated power. Compared to the fixed speed induction generators, the DFIG offers several advantages such as increased power capture, four-quadrant converter topology which lets the decoupled and fast active and reactive power control and reduced mechanical stresses [4,7,8]. The schematic of a DFIG-based wind energy conversion system is depicted in Fig. 1.

While the rotor current vector control is known as the conventional technique to control the DFIG [7,9–11], it suffers from some major drawbacks such as the need for many transformations among different reference frames in the control structure, the requirement of an exact estimation of machine parameters and stability problems if the rotor current PI controllers are not designed wisely.

Nowadays, direct control techniques for the DFIG have found a lot of interests due to their simplicity and high dynamic performances. (Direct torque control) DTC was first introduced in the middle of 1980s [12,13]. The DTC directly controls the developed torque by the machine with the use of torque and flux information and selects the best voltage vector using a switching table [12], a direct self-control [13], a (space vector modulation) SVM [14], a (discrete space vector modulation) DSVM [15] or a fuzzy logic system [16]. In Ref. [17], the fuzzy and DSVM are combined and gained a good performance for direct torque control of the induction machine.

Based on the DTC technique, the (direct power control) DPC was proposed for three phase (pulse width modulation) PWM converters and proven to have many advantages compared to the conventional vector control technique. These advantages include simplicity, fast dynamics and robustness against parameters

* Corresponding author. Tel.: +98 2164543346.
E-mail addresses: m_pichan@yahoo.com (M. Pichan), rastegar@aut.ac.ir (H. Rastegar), m.monfared@um.ac.ir (M. Monfared).

0360-5442/$ – see front matter © 2013 Elsevier Ltd. All rights reserved.
http://dx.doi.org/10.1016/j.energy.2012.12.047

Nomenclature

θ	phase angle between the rotor and stator flux vectors.
ω_s, ω_r, ω_{slip}	synchronous, rotor and slip angular frequencies.
φ_s, φ_r	stator and rotor flux vectors.
I_s, I_r	stator and rotor current vectors.
L_m	mutual inductance.
$L_{\sigma s}$, $L_{\sigma r}$	stator and rotor leakage inductances.
L_s, L_r	stator and rotor self-inductances.
R_s, R_r	stator and rotor resistances.
P_s, Q_s	stator active and reactive powers.
V_s, V_r	stator and rotor voltage vectors.

Superscripts

s	synchronous reference frame.
r	rotor reference frame.
$*$	reference value.
$\hat{}$	conjugate complex.

Subscripts

$\alpha-\beta$	$\alpha-\beta$ axis.
s, r	stator, rotor.
d, q	synchronous $d-q$ axis.

variations and grid voltage disturbances [18–20]. In DPC, the converter switching states are selected from a switching table, based on the error between the reference and measured values of active and reactive powers and the angular position of the ac voltage [18,19] or the virtual flux [20]. Recently, the DPC is proposed for the control of ac motors [21] and more recently DFIGs [22,23]. Although this technique is simple and robust against parameters variations, but the converter switching frequency widely varies as a function of variations of the active and reactive powers, the machine speed and the hysteresis bandwidth. Some solutions have been proposed to fix the converter switching frequency [23,24]. However these methods are based on the stator flux orientation and have complex algorithms which make them inefficient for practical implementations. In Ref. [25], fuzzy and DSVM are combined to minimize the power ripples, however this is also based on the stator flux orientation not stator voltage orientation and uses a switching table. Furthermore it has so much rules and a high switching frequency is needed to effectively reduce the power ripples.

In this paper, at first, a descretized model for the DFIG in the synchronous reference frame is derived. Afterwards, the (fuzzy-based direct power control) FDPC and the (fully fuzzy-based direct power control) FFDPC strategies for the DFIG are proposed. Power errors and their integrations are used as (fuzzy logic controller) FLC inputs. In the FDPC, the output of the FLC is added to proper feed forward terms to generate the reference rotor voltages, while in FFDPC, the rotor voltages are directly generated by the FLC. In both techniques, the obtained reference values for the rotor voltages are then fed to the PWM modulator.

Fuzzy logic controller has been used with success in wind energy conversion systems [26,27]. It is generally accepted that the FLC has the following advantages:

- it does not require the exact model of the process,
- it does not require precise sensors,
- it is robust against noises,
- and it is simple to implement.

These advantages are also expected for the proposed control strategies. The first proposed DPC technique, called FDPC, directly controls the active and reactive powers based on the FLC combined with the measured active and reactive powers, the stator voltage and the rotor speed. Unlike the FDPC, the FFDPC only needs information about the measured active and reactive powers which makes it a simple control strategy. In the proposed methods, the PI controllers, the hysteresis comparators and the switching table are eliminated. Also they are based on the stator voltage orientation which makes them simpler because the stator flux is the integration of stator voltage under normal grid conditions. The switching frequency in the proposed methods is constant and low compared to the switching table based DPC, which brings easier design and practical implementation. Extensive simulations confirm the effectiveness of the proposed control techniques.

2. Principles of the proposed active and reactive power controls

2.1. Mathematical model of the DFIG in the synchronous reference frame

The equivalent circuit of the DFIG in the synchronous reference frame rotating at the speed of ω_s is depicted in Fig. 2, where ω_s is the synchronous angular speed.

The stator and rotor voltage equations in the synchronous reference frame are as

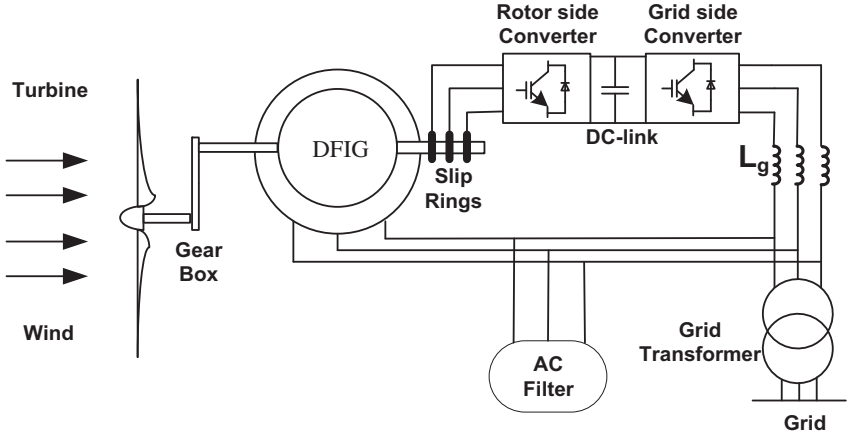

Fig. 1. Schematic of a DFIG-based wind energy conversion system.

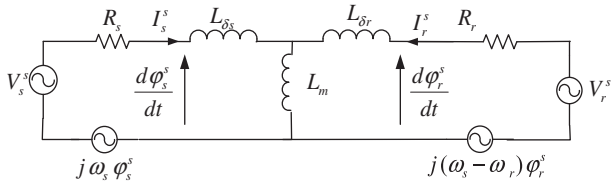

Fig. 2. DFIG equivalent circuit in the synchronous reference frame.

$$V_s^s = R_s I_s^s + \frac{\mathrm{d}\varphi_s^s}{\mathrm{d}t} + j\omega_s\varphi_s^s \tag{1}$$

$$V_r^s = R_r I_r^s + \frac{\mathrm{d}\varphi_r^s}{\mathrm{d}t} + j(\omega_s - \omega_r)\varphi_r^s \tag{2}$$

$$\varphi_s^s = L_s I_s^s + L_m I_r^s \tag{3}$$

$$\varphi_r^s = L_m I_s^s + L_r I_r^s \tag{4}$$

From equations (3) and (4) the stator current in the synchronous reference frame is given by

$$I_s^s = \frac{L_r\varphi_s^s - L_m\varphi_r^s}{L_s L_r - L_m^2} = \frac{\varphi_s^s}{\sigma L_s} - \frac{L_m\varphi_r^s}{\sigma L_s L_r} \tag{5}$$

where $L_s = L_{\delta s} + L_m$ and $L_r = L_{\delta r} + L_m$ and $\sigma = (L_s L_r - L_m^2)/L_m^2$ is the leakage factor.

The active and reactive powers injected to the grid are given by

$$P_s + jQ_s = -\frac{3}{2}V_s^s \times I_s^s \tag{6}$$

Under ideal grid voltages, the amplitude and the rotating speed of the stator flux are constant, consequently $\mathrm{d}\varphi_s^s/\mathrm{d}t = 0$. Accordingly, by neglecting the stator resistance, the stator voltage vector equation of (1) simplifies to

$$V_s^s = j\omega_s\varphi_s^s \tag{7}$$

If the d-axis of the synchronous reference frame is aligned to the stator voltage vector, equation (7) results in

$$\varphi_{\mathrm{sd}} = 0, \varphi_{\mathrm{sq}} = -V_{\mathrm{sd}}/\omega_s \tag{8}$$

Substituting equations (5) and (8) in equation (6) and doing some simple manipulations, the stator active and reactive powers are calculated as

$$P_s = K_\sigma V_{\mathrm{sd}}\varphi_{\mathrm{rd}} \tag{9}$$

$$Q_s = -K_\sigma V_{\mathrm{sd}}\left(\frac{L_r}{L_m}\cdot\frac{V_{\mathrm{sd}}}{\omega_s} + \varphi_{\mathrm{rq}}\right) \tag{10}$$

where $K_\sigma = (3/2)(L_m/\sigma L_s L_r)$.

Since under balanced grid conditions, the stator voltage amplitude remains constant, the power equations of (9) and (10) imply that the active and reactive powers injected to the grid can be effectively controlled by regulating the rotor flux components φ_{rd} and φ_{rq}, respectively.

2.2. Active and reactive power control by adjusting the rotor flux vector

Equation (2) is rearranged and descritized in each small sampling period T_s as follows

$$\frac{\mathrm{d}\varphi_r^s}{\mathrm{d}t} = \frac{\varphi_r^s(k+1) - \varphi_r^s(k)}{T_s} = V_r^s(k) - R_r I_r^s(k) - j(\omega_s - \omega_r)\varphi_r^s(k) \tag{11}$$

After decomposing the above result into d and q components and neglecting the rotor resistance effect, the rotor flux components at the sampling point $(k+1)$ are obtained as

$$\varphi_{\mathrm{rd}}(k+1) = \varphi_{\mathrm{rd}}(k) + T_s V_{\mathrm{rd}}(k) + T_s(\omega_s - \omega_r)\varphi_{\mathrm{rd}}(k) \tag{12}$$

$$\varphi_{\mathrm{rq}}(k+1) = \varphi_{\mathrm{rq}}(k) + T_s V_{\mathrm{rq}}(k) - T_s(\omega_s - \omega_r)\varphi_{\mathrm{rd}}(k) \tag{13}$$

Equations (9) and (10) can be updated with above flux equations to give the active and reactive powers at the sampling point $(k+1)$.

$$P(k+1) = k_\delta V_{\mathrm{sd}}(k)\varphi_{\mathrm{rd}}(k+1) \tag{14}$$

$$Q(k+1) = -k_\delta V_{\mathrm{sd}}(k)\left[\frac{L_r}{L_m}\cdot\frac{V_{\mathrm{sd}}(k)}{\omega_s} + \varphi_{\mathrm{rq}}(k+1)\right] \tag{15}$$

The aim of the control system is to bring the above active and reactive powers to the reference values available at the sampling point (k), i.e.

$$P_{\mathrm{ref}}(k) = P(k+1) \tag{16}$$

$$Q_{\mathrm{ref}}(k) = Q(k+1) \tag{17}$$

Substituting equations (12), (13), (16) and (17) into equations (14) and (15), the reference values for the rotor voltages in the synchronous reference frame are calculated as

$$V_{\mathrm{rd}}(k) = \frac{P_{\mathrm{ref}}(k) - P(k)}{T_s K_\delta V_{\mathrm{sd}}(k)} + \frac{\omega_s - \omega_r}{K_\delta V_{\mathrm{sd}}(k)}Q(k) + \frac{(\omega_s - \omega_r)L_r}{L_m\omega_s}V_{\mathrm{sd}}(k) \tag{18}$$

$$V_{\mathrm{rq}}(k) = -\frac{Q_{\mathrm{ref}}(k) - Q(k)}{T_s K_\delta V_{\mathrm{sd}}(k)} + \frac{\omega_s - \omega_r}{K_\delta V_{\mathrm{sd}}(k)}P(k) \tag{19}$$

3. Proposed direct active and reactive power control strategies

3.1. (Fuzzy-based direct power control) FDPC

Carefully considering equations (18) and (19), these equations can be rewritten as follows

$$V_{\mathrm{rd}} = U_{\mathrm{rd}} + E_{\mathrm{rd}} \tag{20}$$

$$V_{\mathrm{rq}} = U_{\mathrm{rq}} + E_{\mathrm{rq}} \tag{21}$$

where

$$U_{\mathrm{rd}} = k_p\left(P_{\mathrm{ref}} - P\right) \tag{22}$$

$$U_{\mathrm{rq}} = -k_q\left(Q_{\mathrm{ref}} - Q\right) \tag{23}$$

$$E_{\mathrm{rd}} = \omega_{\mathrm{slip}}\left(\frac{Q(k)}{k_\delta V_{\mathrm{sd}}(k)} + \frac{L_r V_{\mathrm{sd}}(k)}{L_m\omega_s}\right) \tag{24}$$

$$E_{\mathrm{rq}} = \omega_{\mathrm{slip}}\frac{P(k)}{k_\delta V_{\mathrm{sd}}(k)} \tag{25}$$

Based on equations (20)–(25), it can be concluded that the rotor reference voltages are composed of two components. The first term in equations (20) and (21), U_{rdq}, is the output of the proportional

power controller, where k_p and k_q are the controllers gains. The second term, E_{rdq}, represents the equivalent rotor back electromagnetic force which is proportional to the slip angular frequency $\omega_{slip} = \omega_s - \omega_r$.

In this paper and based on the above discussion, the (fuzzy logic controller) FLC is used to generate the U_{rdq} term instead of the simple proportional controller, mainly because of two reasons. First, it does not require any mathematical model of the system under control. Second, it is widely accepted that the structure of FLC is simple and easy for practical implementations. The E_{rdq} term is added to the output of the FLC to improve the controller performance in terms of the required control effort and the transient performance. The simplified structure of the fuzzy-based direct power control of doubly-fed induction generator is depicted in Fig. 3.

3.2. (Fuzzy logic controller) FLC

As shown in Fig. 3, power errors (e_p and e_q) and the integration of power errors ($\int e_p$ and $\int e_q$) are used as inputs to the FLC. The output of the FLC is the proper rotor voltage U_{rdq} which is then added to the equivalent rotor back emf, E_{rdq} to generate the rotor reference voltages. Two independent FLCs are used to control active and reactive powers. For all inputs and outputs, seven fuzzy sets are chosen which are (negative big) NB, (negative medium) NM, (negative small) NS, (zero) Z, (positive small) PS, (positive medium) PM and (positive big) PB. For example, the fuzzy set of the active power is depicted in Fig. 4. The range of variations of these variables is dependent on the operating point of the DFIG.

There are 49 rules that form the knowledge repository of the FLC which are used to decide the appropriate control action. These rules are presented in Table 1. A sample rule of the FLC can be written as

$$\text{if}\,(e_p(e_q)\text{is}\,x)\,\text{AND}\left(\int e_p\left(\int e_q\right)\text{is}\,y\right)\text{then}\,(U_{\text{rd}}(U_{\text{rq}})\text{is}\,w).$$

The performance of the fuzzy system is based on Mamdani's min–max rule [28,29]. When a set of input variables is read, each rule is fired. For example, for the FLC of active power, the output of ith rule is

$$\alpha_i = \min\left\{\mu_p(e_p), \mu_{\int p}\left(\int e_p\right)\right\}$$

where μ_p and $\mu_{\int p}$ are the membership functions of each input and α_i is the weighting factor (firing strength) of ith rule. Afterwards, this value should be compared with the membership function of output in the ith rule, thus

$$O_i = \min\{\alpha_i, \mu_{vi}\}$$

where μ_{vi} and O_i are the output membership function and the final membership value of ith rule, respectively. To complete the Mamdani's min–max rule, the maximum value of the final membership values of rules should be chosen. Based on this principle, the output that has maximum possibility distribution is chosen as the output. Thus we can write

$$\mu_v = \max\{O_i\} \quad i = 1, 2, \ldots$$

Finally, the defuzzification method is used to generate the output voltage. Basically, defuzzification is a mapping from a space of fuzzy control actions defined over an output universe of discourse into a space of nonfuzzy (crisp) control actions. It is employed because in many practical applications, a crisp control action is required. Consequently, the complete schematic of the proposed FDPC is depicted in Fig. 5.

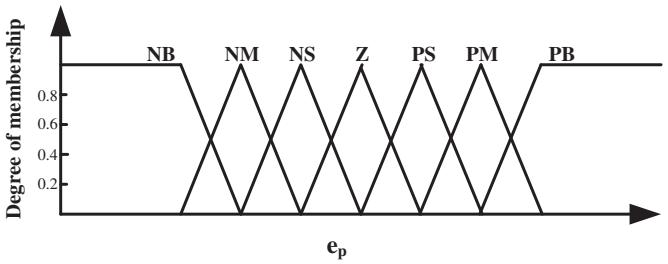

Fig. 4. Fuzzy set of the active power error.

3.3. (Fully fuzzy-based direct power control) FFDPC

According to equations (20) and (21), the rotor voltages are composed of two components. The second term in equations (20) and (21), E_{rdq}, is the equivalent rotor back emf which depends on the active and reactive powers, the stator voltage and some machine parameters. In other words, it is like a feed forward term which improves the overall dynamic performance of the DFIG. Based on equations (24) and (25), since this term is proportional to the slip angular frequency, it will become zero at the synchronous speed. In the (fully fuzzy-based direct power control) FFDPC of DFIG, this term is omitted and only the fuzzy logic controller is used to produce the desired rotor reference voltages. The inputs and outputs of the FFDPC are the same as the FDPC and only the range of the output voltage in the horizontal axis is different. The schematic diagram of the FFDPC is depicted in Fig. 6. As it can be seen, compared to the block diagram of Fig. 5, the E_{rdq} calculation block is removed which makes it simpler to design and implement.

In both techniques, once the rotor voltages are calculated, these voltages must be transformed to the rotor reference frame. This is achieved by the following equation

$$V_r^r = V_r^s e^{j(\omega_s - \omega_r)t} \tag{26}$$

It is worth mentioning that there is no need for a reference voltage limiter or saturation block, since the FLC inherently limits the generated reference voltages at transients. Once V_r^r is

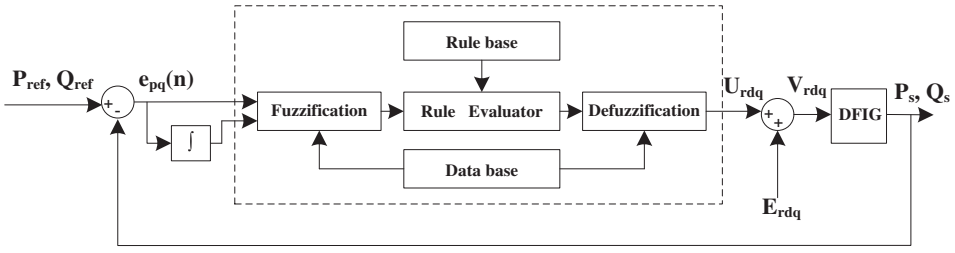

Fig. 3. Structure of FDPC method.

Table 1
FLC rule base.

e	$\int e$						
	PB	PM	PS	Z	NS	NM	NB
PB	PB	PB	PB	PB	PM	PS	Z
PM	PB	PB	PB	PM	PS	Z	NS
PS	PB	PB	PM	PS	Z	NS	NM
Z	PB	PM	PM	Z	NM	NM	NB
NS	PM	PS	Z	NS	NM	NB	NB
NM	PS	Z	NS	NM	NB	NB	NB
NB	Z	NS	NM	NB	NB	NB	NB

calculated, advanced pulse width modulation techniques such as SPWM (sinusoidal pulse width modulation), SVPWM (space vector pulse width modulation), etc. can be used to generate the gating pulses with a fixed switching frequency.

4. Simulations

To investigate the performance of the proposed control strategies under different conditions, extensive simulations are conducted using Matlab/Simulink software. The basic configuration of the simulated system is shown in Fig. 7.

The DFIG is rated at 2 MW and the system parameters are given in Table 2. The (rotor side converter) RSC controls the DFIG's stator active and reactive powers. The (grid side converter) GSC is

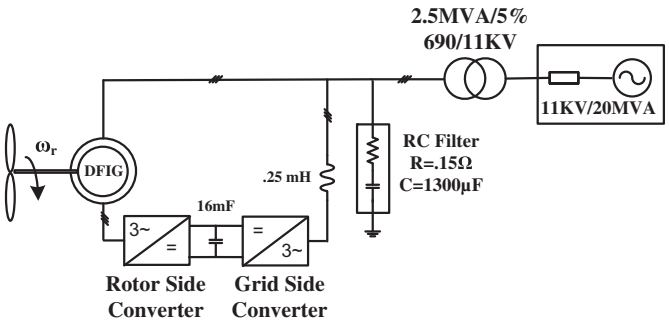

Fig. 7. Configuration of the simulated system.

responsible for balancing the power exchange between the rotor and the grid through maintaining a constant DC-link voltage. So, the GSC is controlled by the same methods used in VSC (voltage source converter) transmission systems [30] or grid-connected rectifiers [31]. In this paper, the proposed method in Ref. [31] with the switching frequency of 5 kHz is used for GSC. The DC-link voltage is set to 1200 V. A high frequency RLC filter is connected to the stator side to suppress the switching harmonics and high frequency noises generated by the two converters. During the simulations, the sampling period was set to 250 μs. To generate the switching pulses, the (space vector modulation) SVM technique with the switching frequency fixed at 2 kHz is utilized. The range of

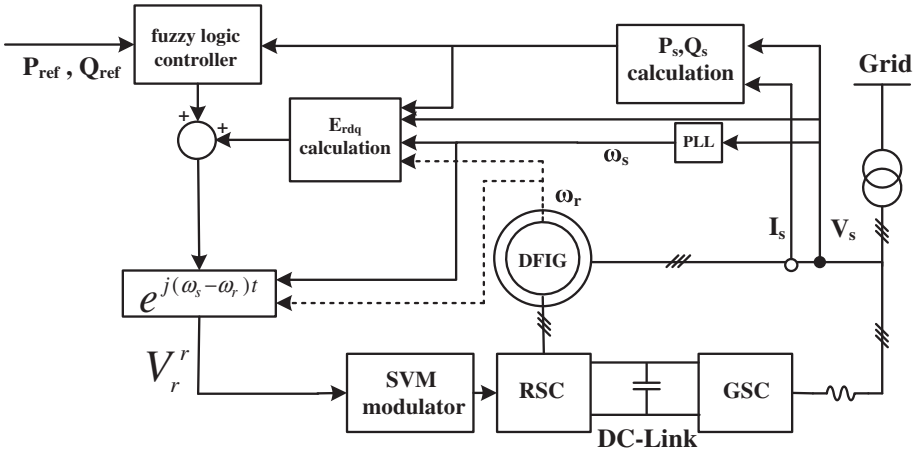

Fig. 5. Schematic of the proposed FDPC for DFIG.

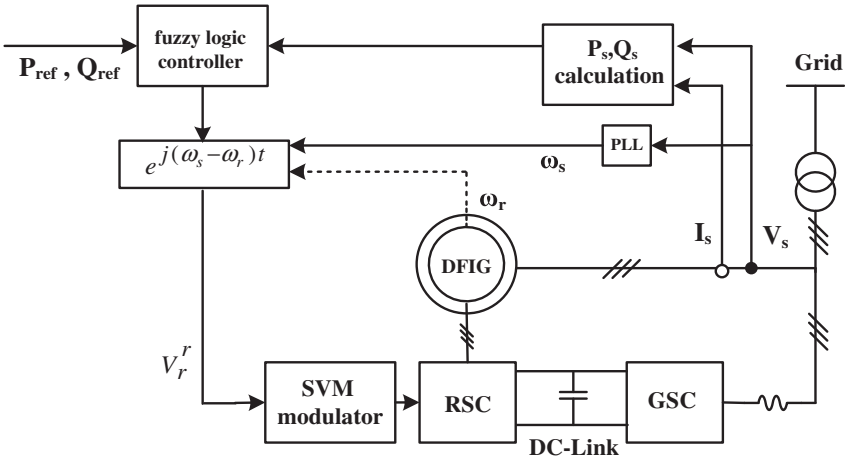

Fig. 6. Schematic of the proposed FFDPC for DFIG.

Table 2
Parameters of the simulated DFIG.

Rated power	2 MW
Stator voltage	690 V
Stator/rotor turns ratio	0.3
R_s	0.0108 pu
R_r	0.0121 pu(referred to the stator)
L_m	3.362 pu
$L_{\sigma s}$	0.102 pu
$L_{\sigma r}$	0.11 pu(referred to the stator)
Lumped inertia constant	0.2 s
Number of pole pairs	2

Table 3
The range of membership functions.

	FDPC		FFDPC	
	Min	Max	Min	Max
e_p	$-5e+5$	$5e+5$	$-5e+5$	$5e+5$
$\int e_p$	$-5e+5$	$5e+5$	$-5e+5$	$5e+5$
e_q	$-5e+5$	$5e+5$	$-5e+5$	$5e+5$
$\int e_q$	$-5e+5$	$5e+5$	$-5e+5$	$5e+5$
U_{rd}	−170	170	−180	180
U_{rq}	−75	75	−80	80

fuzzy sets in the horizontal axes for both proposed methods are given in Table 3.

4.1. Steady-state and dynamic performances

During the simulations, at first, the grid side converter is activated to make and fix the DC-link voltage. Afterwards, the stator is energized at constant rotor speed. Finally, the rotor side converter is activated to bring the stator active and reactive powers to the reference values. The final step is only shown in the following and the two first steps are not displayed.

The performance of the proposed FDPC and FFDPC strategies in the steady-state condition is shown in Fig. 8. For both strategies, the active and reactive power references are set to 2 MW and −0.5 MVar, respectively ('−'indicates absorbing the reactive power). The rotor speed is set externally to 1.2 pu, where the synchronous speed is defined as 1 unit. According to Fig. 8, the effectiveness of the proposed strategies is confirmed with precise power control, minimum current distortions, less harmonic noises and at the same time, more accurate regulation and fewer ripples in the output active and reactive powers. The THD (total harmonic distortion) of stator current is 1.42% and 1.44% for FDPC and FFDPC, respectively.

In another study, various step changes in the active and reactive power references are applied to evaluate the dynamic performance of the proposed DPC strategies. The results for both FDPC and FFDPC strategies are shown in Fig. 9 for rotor speed of 1 pu. Initially the rotor side converter is enabled with the active and reactive power references at 0 MW and −0.5 MVar, respectively. Then the active and reactive power references jumped from 0 to 2 MW at 0.2 s and from −0.5 to 0.5 MVar at 0.4 s, respectively. After that, step fall of active power reference from 2 MW to 1 MW at 0.6 s is applied to evaluate both rising and falling performances. Both proposed control strategies exhibit a fast dynamic response and the active and reactive powers track the reference values within a few milliseconds with almost no coupling effects and transient oscillations.

The transient performances of proposed strategies in terms of rising and falling times of active and reactive powers are compared in Table 4. As it was expected, while both techniques offer a very fast transient performance, the FDPC can achieve a slightly faster transient response, mainly due to the feed forward path in its structure. Due to the fast nature of both DPCs, a decoupled control of active and reactive powers is also achieved, which is obvious in Fig. 9.

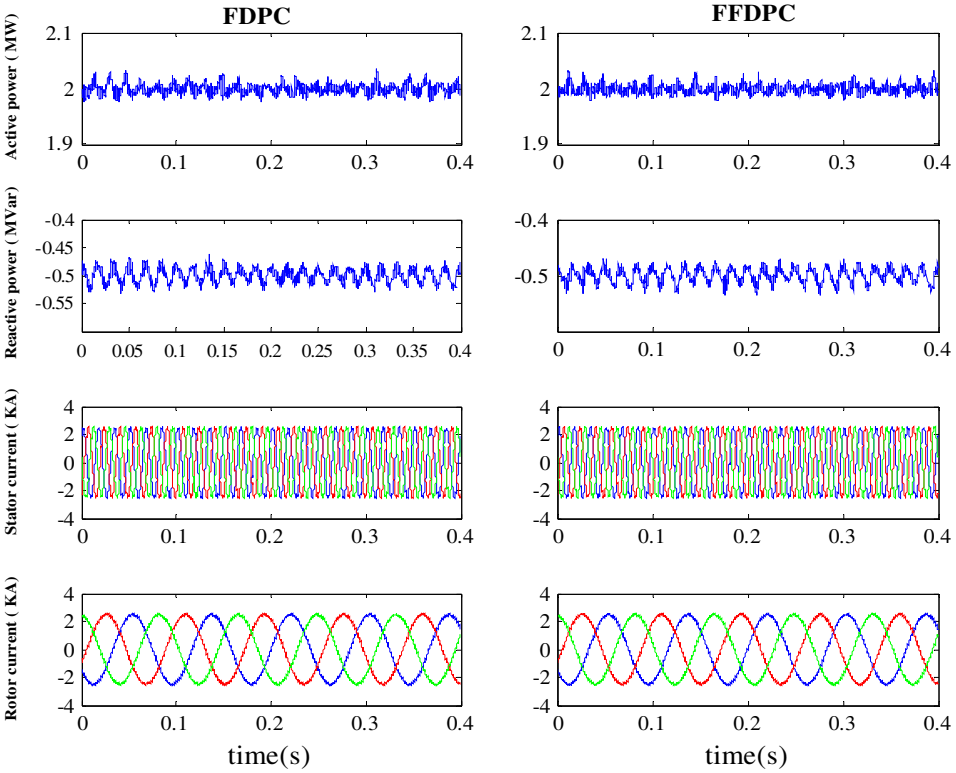

Fig. 8. Steady-state performance of the proposed DPC strategies at rotor speed of 1.2 pu.

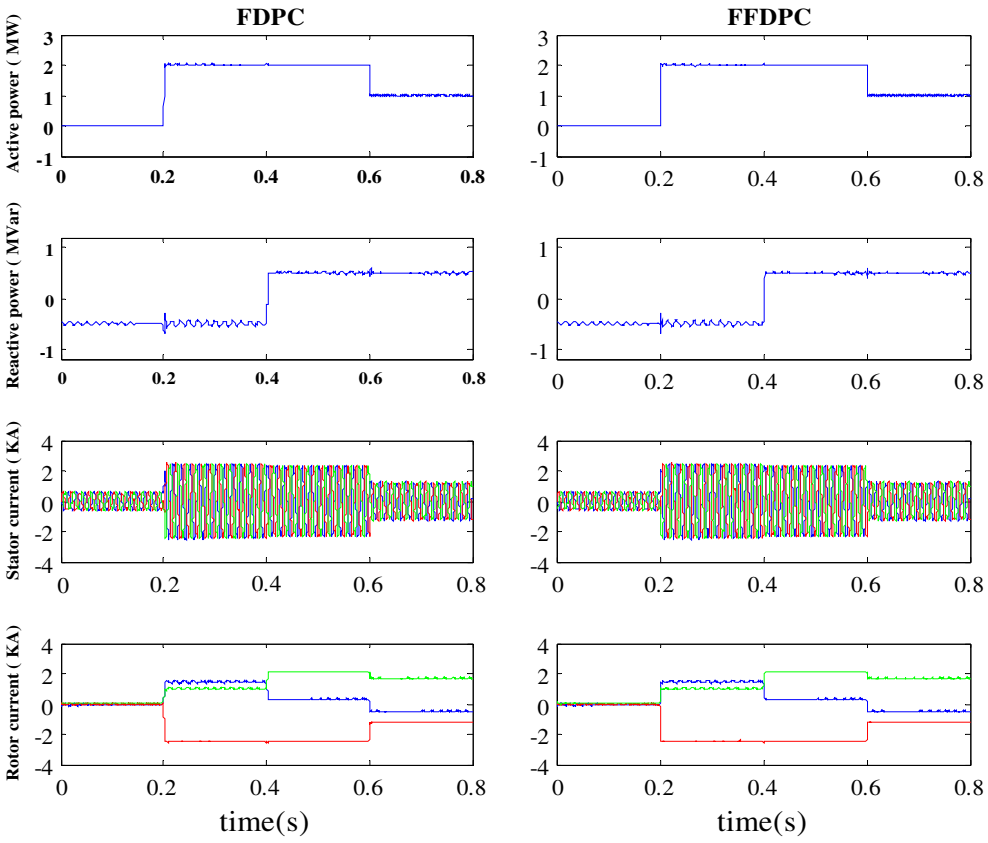

Fig. 9. Transient performance of the proposed DPC strategies under various active and reactive power step changes at rotor speed of 1 pu.

4.2. Impact of parameters mismatch

As mentioned above, since the FLC does not require any mathematical model of the controlled process, it is not almost affected by model parameter variations. Based on equations (24) and (25), in the proposed methods, only FDPC uses some DFIG parameters which are k_σ and L_r/L_m ratio. Since the leakage flux magnetic path is mainly in the air, so the variations of the leakage inductances ($L_{\sigma s}$ and $L_{\sigma r}$) during the operation are not considerable and can be safely neglected. These parameters can be simplified as

$$k_\sigma \approx \frac{3}{2}\frac{1}{L_{\sigma s}+L_{\sigma r}}, \frac{L_r}{L_m} = 1+\frac{L_{\sigma r}}{L_m} \approx 1 \tag{27}$$

Based on equation (27), it can be concluded that the effect of DFIG parameters variations is negligible. To confirm the above analysis, a simulation study with 40% mismatch in the mutual inductance value is done. The results are depicted in Fig. 10 which proves the analytical achievements.

4.3. Operation under network voltage distortions

Sometimes wind farms with DFIGs are connected to weak grids at remote locations where voltage distortions are likely to happen. This may result in deteriorated performance or even instability of grid interfacing converters in some cases.

To examine the performance of the proposed control strategies under grid voltage distortions, a simulation was done with 5th and 7th harmonic components injected into the grid voltages, as shown in equation (28).

$$\begin{aligned} V_{sa} &= V_m\sin(\omega t)+k_1V_m\sin(5\omega t)+k_2V_m\sin(7\omega t)\\ V_{sb} &= V_m\sin\left(\omega t-\frac{2\pi}{3}\right)+k_1V_m\sin\left(5\omega t+\frac{2\pi}{3}\right)+k_2V_m\sin\left(7\omega t-\frac{2\pi}{3}\right)\\ V_{sc} &= V_m\sin\left(\omega t+\frac{2\pi}{3}\right)+k_1V_m\sin\left(5\omega t-\frac{2\pi}{3}\right)+k_2V_m\sin\left(7\omega t+\frac{2\pi}{3}\right) \end{aligned} \tag{28}$$

Table 4
Comparison of transient performances.

	Active power rising time (ms)	Active power falling time (ms)	Reactive power rising time (ms)
FDPC	3.1	2	3.8
FFDPC	3.5	2	4

For different values of k_1 and k_2, the power error and ripple, calculated from equation (29) are reported in Table 5.

$$\Delta S(\%) = \sqrt{\frac{\Delta P^2+\Delta Q^2}{P_{\text{ref}}^2+Q_{\text{ref}}^2}}\times 100 \tag{29}$$

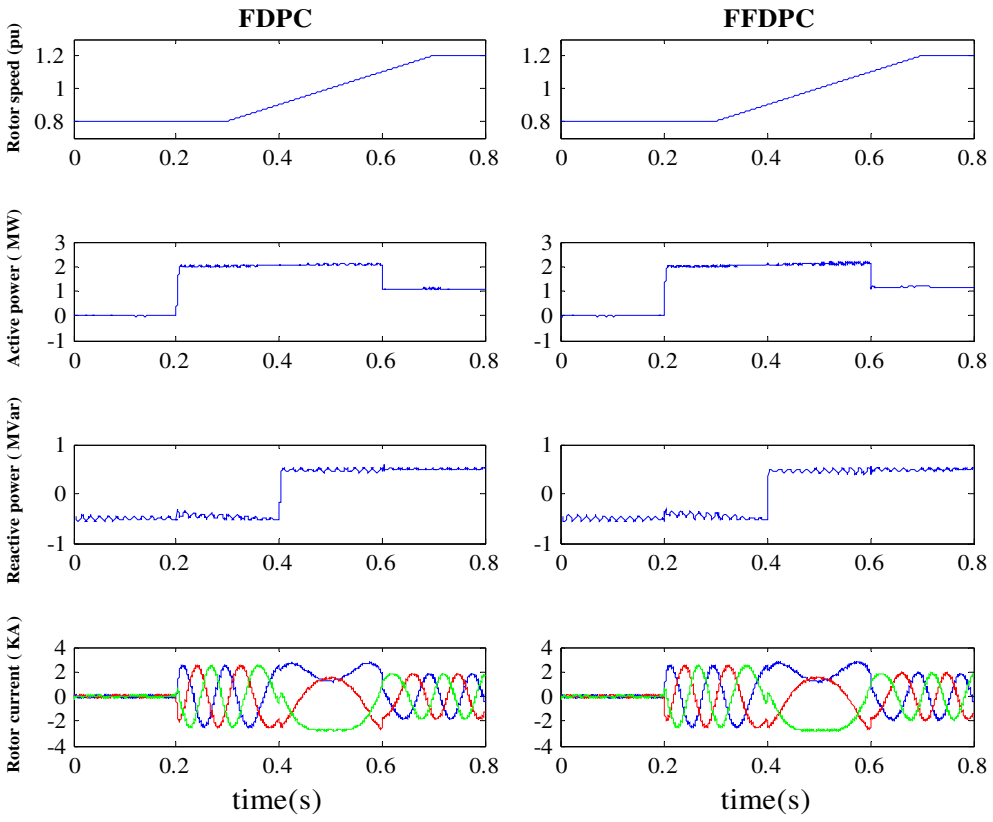

Fig. 10. Simulated results under various stator active and reactive power steps and rotor speed variations with 40% mismatch in L_m.

Both control strategies maintain their normal operation. Since the network voltage is harmonically distorted, the calculated powers are not constant and have a ripple which is a little larger in the case of FDPC. These results were expected, because the FDPC technique includes the feed forward terms in its control structure which are closely related to the quality of the measured grid voltages.

4.4. Operation under imbalanced network voltages

Considering positive and negative sequence components, network voltages are defined by

$$\begin{aligned} V_{sa} &= V_m\sin(\omega t) + k_3 V_m \sin(\omega t) \\ V_{sb} &= V_m\sin\left(\omega t - \frac{2\pi}{3}\right) + k_3 V_m \sin\left(\omega t + \frac{2\pi}{3}\right) \\ V_{sc} &= V_m\sin\left(\omega t + \frac{2\pi}{3}\right) + k_3 V_m \sin\left(\omega t - \frac{2\pi}{3}\right) \end{aligned} \tag{30}$$

Under imbalanced network voltage conditions, the quality of the (phase locked loop) PLL mainly determines the control strategy's performance. In this work, a simple arctan function is used to calculate the line voltage angular position from its $\alpha\beta$ components for both methods. As shown in Table 5, the imbalanced voltages increase the power ripples. It should be noted that since the FFDPC does not need direct information of grid voltages, it is more immune against the grid voltage disturbances as presented in Table 5.

Table 5
Power ripple $\Delta s\%$ as a function of 5th and 7th harmonic amplitudes and voltage imbalance ($P_{ref} = 2$ MW, $Q_{ref} = -0.5$ MVar).

k_1	k_2	k_3	FDPC	FFDPC
0	0	0	2.17	2.17
0.03	0.01	0	10.85	9.94
0.05	0.03	0	25.32	24.69
0	0	0.01	5.42	5.12
0	0	0.03	14.4	14.13

5. Conclusion

Two new direct active and reactive power control strategies for a DFIG-based wind energy conversion system, based on the (fuzzy logic controller) FLC are proposed in this paper: the FDPC and the FFDPC. The FFDPC directly calculates the rotor reference voltages from the instantaneous power errors using an FLC, while in the FDPC, proper feed forward terms are added to the FLC outputs to improve the dynamic performance. The control structures of proposed methods are simple and also these methods are based on stator voltage orientation rather than stator flux orientation. The harmonic filter and the converter design is easy because of the constant switching frequency. Simulation results confirm the effectiveness of the proposed methods under transient and steady state conditions. Furthermore, the simulated performance of both methods under harmonically distorted and imbalanced grid voltages show that they can successfully maintain their normal operation, with just increased power ripples which are more evident for the FDPC.

References

[1] Ozbek M, Rixen DJ, Erne O, Sanow G. Feasibility of monitoring large wind turbines using photogrammetry. Energy 2010;35:4802–11.
[2] Sawetsakulanond B, Kinnares V. Design, analysis, and construction of a small scale self-excited induction generator for a wind energy application. Energy 2010;35:4975–85.

[3] Mabel MC, Raj RE, Fernandez E. Adequacy evaluation of wind power generation systems. Energy 2010;35:5217–22.
[4] Fernandez LM, Garcia CA, Jurado F. Comparative study on the performance of control systems for doubly fed induction generator (DFIG) wind turbines operating with power regulation. Energy 2008;33:1438–52.
[5] Melício R, Mendes VMF, Catalão JPS. Comparative study of power converter topologies and control strategies for the harmonic performance of variable-speed wind turbine generator systems. Energy 2011;36:520–9.
[6] Pouresmaeil E, Bellmunt OG, Miracle DM, Jané JB. Multilevel converters control for renewable energy integration to the power grid. Energy 2011; 36:950–63.
[7] De Doncker RW, Muller S, Deicke M. Doubly fed induction generator systems for wind turbines. IEEE Ind Appl Mag 2002;8:26–33.
[8] Fernandez LM, Garcia CA, Jurado F. Operating capability as a PQ/PV node of a direct-drive wind turbine based on a permanent magnet synchronous generator. Renew Energ 2010;35:1308–18.
[9] Akagi H, Sato H. Control and performance of a doubly-fed induction machine intended for a flywheel energy storage system. IEEE Trans Power Electron 2002;17:109–16.
[10] Pena R, Clare JC, Asher GM. Doubly fed induction generator using back-to-back PWM converters and its application to variable-speed wind-energy generation. Inst Elect Eng Proc Elect Power Appl 1996;143:231–41.
[11] Song Z, Shi T, Xia C, Chen W. A novel adaptive control scheme for dynamic performance improvement of DFIG-Based wind turbines. Energy 2012;38: 104–17.
[12] Takahashi I, Noguchi T. A new quick-response and high-efficiency control strategy of an inductionmotor. Inst Elect Eng Trans Ind Appl 1986;22:820–7.
[13] Depenbrock M. Direct self-control (DSC) of inverter-fed induction machine. IEEE Trans Power Electron 1988;3:420–9.
[14] Buja GS, Kazmierkowski MP. Direct torque control of PWM inverter-fed AC motors—a survey. IEEE Trans Ind Electron 2004;51:744–57.
[15] Casadei D, Sera G, Tani A. Implementation of a direct torque control algorithm for induction motors based on discrete space vector modulation. IEEE Trans Power Electron 2000;15:769–77.
[16] Mir SA, Elbuluk ME, Zinger DS. Fuzzy implementation of direct self-control of induction machines. IEEE Trans Ind Appl 1994;30:729–35.
[17] Wei X, Chen D, Zhao C. Minimization of torque ripple of direct-torque controlled induction machines by improved discrete space vector modulation. Electr Power Syst Res 2004;72:103–12.
[18] Noguchi T, Tomiki H, Kondo S, Takahashi I. Direct power control of PWM converter without power-source voltage sensors. IEEE Trans Ind Appl 1998; 34:473–9.
[19] Escobar G, Stankovic AM, Carrasco JM, Galvan E, Ortega R. Analysis and design of direct power control (DPC) for a three phase synchronous rectifier via output regulation subspaces. IEEE Trans Power Electron 2003;18:823–30.
[20] Malinowski M, Kazmierkowski MP, Hansen S, Blaabjerg F, Marques GD. Virtual-flux-based direct power control of three-phase PWM rectifiers. IEEE Trans Ind Appl 2001;37:1019–27.
[21] Luo X. Direct power control of AC motors. Master's thesis, University of Nevada; Reno: 2009. [online]. Available from: http://search.proquest.com/docview/304945410/fulltextPDF/134EBD955116D8DB4AA/1?accountid=45164.
[22] Xu L, Cartwright P. Direct active and reactive power control of DFIG for wind energy generation. IEEE Trans Energy Convers 2006;21:750–8.
[23] Zhi D, Xu L. Direct power control of DFIG with constant switching frequency and improved transient performance. IEEE Trans Energy Convers 2007;22: 110–8.
[24] Abad G, Rodríguez MA, Poza J. Two-level VSC-based predictive direct power control of the doubly fed induction machine with reduced power ripple at low constant switching frequency. IEEE Trans Energy Convers 2008;23:570–80.
[25] Kazemi MV, Moradi M, Kazemi RV. Minimization of powers ripple of direct power controlled DFIG by fuzzy controller and improved discrete space vector modulation. Electr Power Syst Res 2012;89:23–30.
[26] Lin WM, Hong CM, Cheng FS. Fuzzy neural network output maximization control for sensorless wind energy conversion system. Energy 2010;35: 592–601.
[27] Kamel RM, Chaouachi A, Nagasaka K. Wind power smoothing using fuzzy logic pitch controller and energy capacitor system for improvement microgrid performance in islanding mode. Energy 2010;35:2119–29.
[28] Lee CC. Fuzzy logic in control systems: fuzzy logic controller. Part I. IEEE Trans Syst Man Cybern 1990;20:404–18.
[29] Lee CC. Fuzzy logic in control systems: fuzzy logic controller. Part II. IEEE Trans Syst Man Cybern 1990;20:419–35.
[30] Thomas JL, Poullain S, Benchaib A. Analysis of a robust DC-bus voltage control system for a VSC-Transmission scheme. In: Proc. 7th Int. Conf. AC-DC Power Trans; 2001. p. 119–24.
[31] Monfared M, Rastegar H, Kojabadi HM. High performance direct instantaneous power control of PWM rectifiers. Energ Convers Manage 2010;51:947–54.